# Anisotropy in Stratified Shear Turbulence

Joseph Werne* and David C. Fritts
Colorado Research Associates
Boulder, CO 80301

## Abstract

Turbulence in a stratified shear layer is simulated over a range of Reynolds numbers in support of the AirBorne Laser (ABL) project using the DoD Cray T3E's at CEWES and NAVO. Large- and small-scale anisotropy are evaluated for turbulence instigated by the most unstable asymptotic linear Kelvin-Helmholtz (KH) eigenmode. Shear-layer Reynolds numbers as high as $Re = 24,000$ are achieved as the layer expands and small length-scale motions develop. Anisotropy is examined by comparing 1) spectra for the longitudinal and transverse correlation coefficients, 2) RMS velocity components, and 3) velocity and temperature derivatives. The presence of mean shear produces a more nearly axisymmetric, as opposed to isotropic, turbulence; however, departures from axisymmetry due to stratification are evident in the dissipation fields (*i.e.*, at small scales). Anisotropy is most pronounced in regions where the index of refraction is large.

## Introduction

The main objective of the ABL program is to develop adaptive optical systems capable of focusing laser energy on a target through a few hundred kilometers horizontally in the upper troposphere and lower stratosphere. Two facets of the ABL program are currently being carried out with the aid of HPCMO Challenge allocations: optical propagation simulations through modeled stratospheric turbulence directed by Dr. Bill Brown address the design issues associated with the ABL optical system; our companion effort concentrates on improving the understanding of stratospheric turbulence phenomena so that more realistic models may be used for atmospheric-propagation-simulation input. In this report we concentrate on the anisotropy present in horizontally broad but vertically shallow turbulent patches that appear throughout the stratosphere. Future work will address the spacing and intermittent distribution of these patches.

## Sources of Anisotropy in Stratospheric Turbulence

Stratospheric turbulence, like all naturally occurring turbulence phenomena, develops in an anisotropic environment. Wind shear and density stratification establish identifiable directions in the flow fields. The classic interpretation of turbulent motions in terms of a cascade of eddy kinetic energy from large-length-scale motions to smaller scales is often employed with the additional assumption of isotropy at the smallest scales; however, isotropy can exist only if no preferred direction can be identified from the statistical character of the flow fields. Here we quantify departures from isotropy for a turbulent-cascade-inducing event in stratified shear flow. These results are important to ABL design because anisotropy of the underlying medium can produce signatures in laser beam spreading; *e.g.*, initial beams of circular cross-section may become elliptical after passing through a region of strong anisotropy.

## Mixing and Density Gradients

The numerical method and basic evolution of the shear layer have been documented elsewhere (Werne and Fritts 1998, 1999a,b). Current code performance is 105 Mflops/PE.

Fig. 1 communicates some of the main results previously reported and also depicts the mixing dynamics visually via the viscous $\epsilon$ (yellow) and thermal $\chi$ (blue) dissipation rates. $\epsilon = 2\nu s_{ij} s_{ij}$, and $\chi = \partial_i T \partial_i T$, where $s_{ij} = (\partial_i u_j + \partial_j u_i)/2$ is the velocity stress tensor, and $\partial_i$ represents differentiation in the $i$-direction. While $\epsilon$ is large in the interior (indicating intense velocity fluctuations at small spatial scales), $\chi$ peaks in the edge regions. Intense mixing by the interior turbulence reduces thermal fluctuations there, while entrainment in the edge regions maintains large temperature gradients at the edges of the layer. Because variations in the index of refraction $n$ are proportional to temperature fluctuations in the stratosphere, we expect peaks in $n$ at the layer's edges as well. These edge regions exhibit different dynamics and experience a different environment from the mid-layer. Adjustment of the background temperature and shear profiles by turbulent motions result in a dynamically marginal stability profile with $Ri \approx 1/4$ near the edges and a convectively

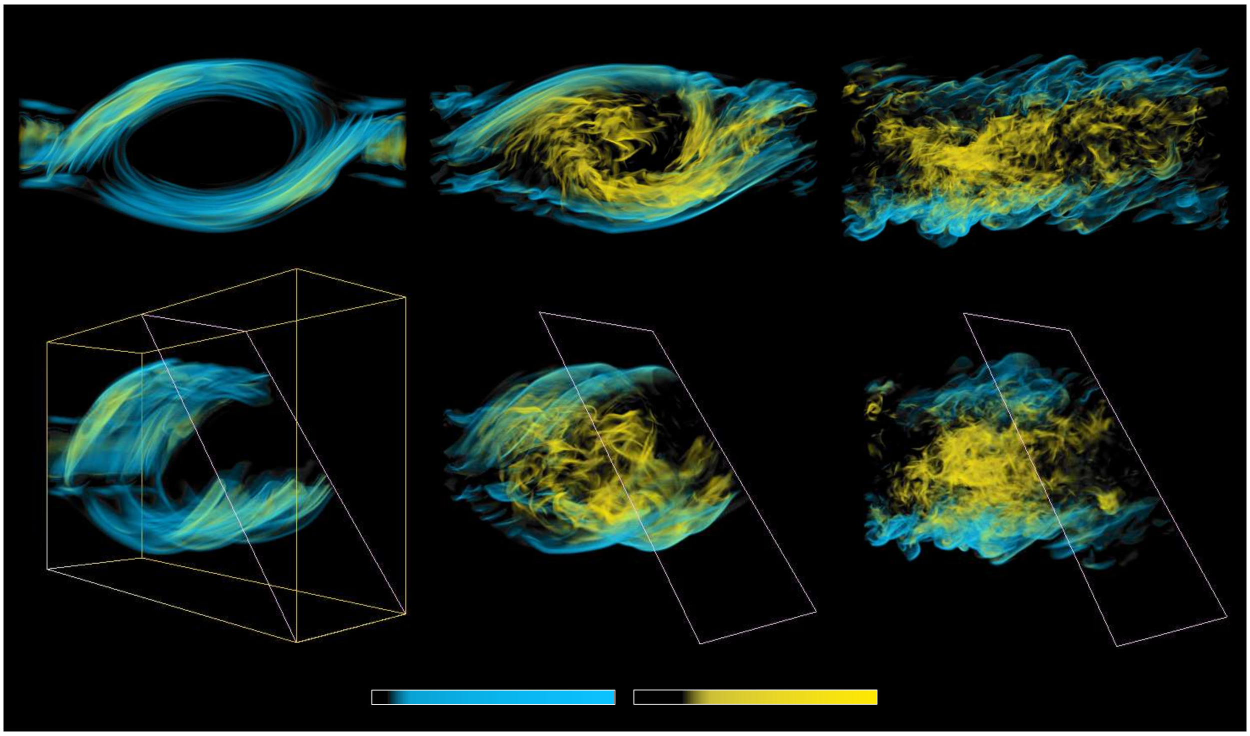

Figure 1: Viscous (yellow) and thermal (blue) dissipation at $t = 66$, 103 and 164, side and perspective views.

marginal stability profile with $Ri \approx 0$ at mid-layer (Werne and Fritts, 1999a). Hence, turbulent kinetic energy is more intense at mid-layer while stratification dominates the edge-region dynamics.

Horizontally expansive (10's of kilometers) of vertically thin (of order 100 $m$) turbulent layers have been observed in the lower stratosphere (Ierkic *et al.*, 1990). High-resolution radar backscatter images obtained at the Arecibo observatory at 2.4 GHz and 20 $m$ vertical resolution exhibit the double-peaked structure of radar reflectivity predicted by $\chi$ in Fig. 1 (Ierkic *et al.*, 1990).

## Spectral Anisotropy

Fig. 2a,b depicts horizontal spectra at mid-layer and in the edge regions of the turbulent layer at time $t = 164$, the same time as that of the right panels in Fig. 1. The $-5/3$ power law (arbitrary normalization) indicates the Kolmogorov prediction for isotropic turbulence. The temperature spectra in the edge regions is enhanced by more than two orders of magnitude, as was reported previously (Werne and Fritts, 1998) and as is consistent with the more intense thermal fluctuations there (see Fig. 1). Fig. 2c,d tests the isotropy of the spectra. Data for the slightly earlier time $t = 146$ is also included so that some sense of the evolution of anisotropy can be gaged. The longitudinal spectra $E_u(k_x)$ (in 2c) and $E_v(k_y)$ (in 2d) for $t = 164$ are identical to those in Fig. 2a,b. Predicted isotropic spectra $E_u(E_v)$ and $E_v(E_u)$ are also included; they are obtained from the transverse spectra $E_v(k_x)$ (in 2c) and $E_u(k_y)$ (in 2d) and the isotropic relation

$$E_1(k_x) = 2k_x \int_{k_x}^{\infty} \frac{E_2(k)}{k^2}\, dk \ , \tag{1}$$

which we deduce upon integrating the better-known form (Hinze, 1959)

$$-2E_2(k_x) = k_x\ \partial_{k_x} E_1(k_x) - E_1(k_x)\ . \tag{2}$$

The figure indicates isotropy to be a good approximation throughout the layer; however, the reader should be warned, comparisons on log-log scales are not critical, and examination of the same spectra on a linear-log

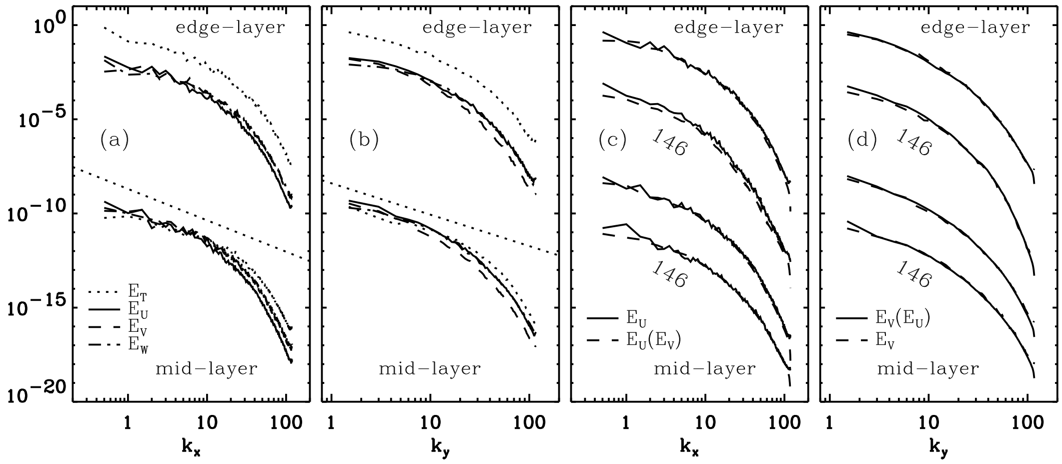


Figure 2: $T$, $u$, $v$ and $w$ spectra versus (a) $k_x$ and (b) $k_y$ at $t = 164$ for $z = 0.0$ and 2.4; $k^{-5/3}$ (dashed) is also shown. Comparison with Eq. 1 for (c) $u$ and (d) $v$ spectra in $k_x$ and $k_y$ at $t = 146$ (labeled) and $t = 164$.

scale (not shown) reveals departures from isotropy from 10% to 80%, depending on the wavenumber. At the earlier time $t = 146$ the spectra in the edge regions are more notably anisotropic, exhibiting deviations of 200% to 300%.

## Dissipation Anisotropy

Simple symmetry arguments and mass conservation (*i.e.*, $\vec{\nabla} \cdot \vec{v} = 0$) are all that is needed to derive Eq. 1. Similarly, symmetry relations for the 2nd-order structure functions for velocity and temperature differences (over separation distance $r$) can also be derived (Monin and Yaglom, 1975). At the smallest spatial scales ($r \rightarrow 0$), the structure functions can be expressed in terms of velocity and temperature derivatives. For example, isotropic flow relations at the smallest scales give

$$\langle \partial_x u \partial_x u \rangle = \langle \partial_y v \partial_y v \rangle \ , \ \langle \partial_x v \partial_x v \rangle = 2 \langle \partial_x u \partial_x u \rangle \ \text{ and } \ \langle \partial_x v \partial_y u \rangle = -\frac{1}{2} \langle \partial_x u \partial_x u \rangle \ . \tag{3}$$

Similar isotropic equations relating other longitudinal, transverse, and cross terms can also be derived, and all the thermal-gradient terms are equal; *i.e.*, $\langle \partial_x T \partial_x T \rangle = \langle \partial_y T \partial_y T \rangle = \langle \partial_z T \partial_z T \rangle$.

Fig. 3a,d demonstrates that these symmetry constraints are too severe for our turbulent shear layer: the left-most profile in Fig. 3a,d overlays all of the velocity-derivative terms (multiplied by 1, 2, or $-0.5$, as appropriate according to Eq. 3) for $t = 146$ (in 3a) and $t = 164$ (in 3d); significant departures from isotropy are evident.

The anisotropy at small scales demonstrated by Fig. 3a,d (left-most curves) should be anticipated, given the presence of stratification and shear. In an attempt to quantify departures from isotropy, we examine relations for axisymmetric (as opposed to isotropic) turbulence, choosing the streamwise direction as the symmetry axis. (This is found to be a better choice than the vertical direction.) Different derivative relationships from those in Eq. 4 hold for axisymmetry (George and Hussein, 1991):

$$\langle \partial_y v \partial_y v \rangle - \langle \partial_x u \partial_x u \rangle = \langle \partial_z w \partial_z w \rangle - \langle \partial_x u \partial_x u \rangle = \langle \partial_y u \partial_x v \rangle - \langle \partial_z v \partial_y w \rangle = \langle \partial_z u \partial_x w \rangle - \langle \partial_z v \partial_y w \rangle \tag{4}$$

$$\langle \partial_y u \partial_x v \rangle = \langle \partial_z u \partial_x w \rangle \ , \ \langle \partial_y u \partial_y u \rangle = \langle \partial_z u \partial_z u \rangle \ , \ \langle \partial_x v \partial_x v \rangle = \langle \partial_x w \partial_x w \rangle \ , \ \langle \partial_z v \partial_z v \rangle = \langle \partial_y w \partial_y w \rangle \tag{5}$$

$$\langle \partial_z T \partial_z T \rangle = \langle \partial_y T \partial_y T \rangle \ . \tag{6}$$

Fig. 3b,e shows the four profiles in Eq. 4. Note that the differences in Eq. 4 measure the degree of anisotropy, since zero values are obtained in the isotropic limit. Also note that the agreement in Fig. 3b,e is actually much better than in the left-most curve of Fig. 3a,d; *i.e.*, curves in 3b,e range over typically

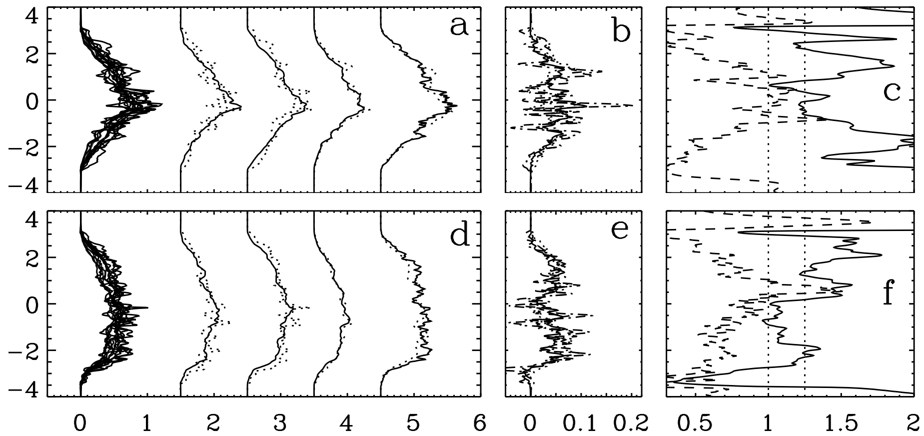


Figure 3: Profiles of dissipation terms with height testing isotropic and axisymmetric relationships for $t = 146$ (a,b,c) and $t = 164$ (d,e,f). (a,d) Left most curve shows all velocity-derivative correlations appearing in the definition of $\epsilon$ (see text). Transverse (cross) terms are multiplied by 0.5 ($-2$); all curves should overlay for perfect isotropy. The remaining four profile pairs in (a,d) to the right test axisymmetry relations (Eq. 5). They are plotted in the order in which the equations appear in Eq. 5; solid curves represent the terms to the left of the equals sign. $\langle \partial_z u \partial_z u \rangle$ and $\langle \partial_x w \partial_x w \rangle$ are multiplied by 1/1.16 (1/1.06) and 1.16 (1.06), respectively, for $t = 146$ ($t = 164$) to reveal the degree to which axisymmetry is violated by buoyancy effects; similarly, $\langle \partial_y w \partial_y w \rangle$ is multiplied by 1.35 (1.12). (b,e) All curves in Eq. 4 are included; no multiplication factors are applied. (c,f) $\chi_y/\chi_x$ (solid) and $\chi_y/\chi_z$ (dashed) versus height; see text for definitions.

0.1, while those in the left-most plot of 3a span roughly 0.6; hence, axisymmetric turbulence seems a better description of the flow than isotropic turbulence.

The remaining curves in Fig. 3a,d probe Eq. 5. While the first relation in Eq. 5 appears satisfactory, the second and third exhibit departures of 16% (6%), and the fourth reveals departures of 35% (12%) at $t = 146$ ($t = 164$). These discrepancies are hidden in the plots by reducing $\langle \partial_z u \partial_z u \rangle$ by the factor 1/1.16 (1/1.06), by compensating $\langle \partial_x w \partial_x w \rangle$ by 1.16 (1.06), and by increasing $\langle \partial_y w \partial_y w \rangle$ by 1.35 (1.12) relative to $\langle \partial_z v \partial_z v \rangle$.

Departures from axisymmetry are expected if stable stratification is significant: suppression of $w$ relative to $u$ and $v$ and of typical vertical length scales $\delta_z$ relative to horizontal scales $\delta_H$ is anticipated if buoyancy influences the motion. If all occurrences of $w$ in Eqs. 4–6 are reduced by $\approx 1.077$ ($\approx 1.03$) and those including $\partial_z$ are increased by 1.077 (1.03), the behavior in Fig. 3a,b,d,e is predicted for $t = 146$ ($t = 164$). Note that this simple characterization of the effects of buoyancy appears better for the earlier time $t = 146$ where the right four pairs of curves in Fig. 3a agree through the full depth of the turbulent layer. For $t = 164$, the correction of 1.03 brings the center portion of the layer into agreement for all of the curves, while near the edges discrepancies persist. Also note that Fig. 3b,e reveals uniform departures of isotropy throughout most of the layer at $t = 146$, while a tendency towards isotropy in the center of the layer is revealed at $t = 164$ while nearer to the edges anisotropy persists.

Fig. 3c,f shows the ratios $\chi_y/\chi_z = \langle \partial_y T \partial_y T \rangle \, / \, \langle \partial_z T \partial_z T \rangle$ (dashed) and $\chi_y/\chi_x = \langle \partial_y T \partial_y T \rangle \, / \, \langle \partial_x T \partial_x T \rangle$ (solid). In the interior of the shear layer $\chi_y/\chi_z \approx 1$ is achieved at $t = 146$, indicating axisymmetry for the fluctuations about the streamwise direction, while at $t = 164$, $\chi_y/\chi_x \approx 1$ near the middle of the layer, indicating the controlling influence of the vertical direction. This behavior indicates the relatively greater influence of buoyancy over shear effects at the later time as the flow begins to restratify. The edge regions at both times exhibit $\chi_y/\chi_z < 1$, demonstrating the reduction of $\delta_z$ due to buoyancy. Hence, stratification is seen to be relatively greater near the edges of the turbulence layer. The increase in $\chi_y/\chi_x$ near the layer's edges at $t = 146$ reflects the relatively intense streamwise-aligned vortex tubes there which enhance (reduce) spanwise (streamwise) gradients for $T$.

## Conclusions

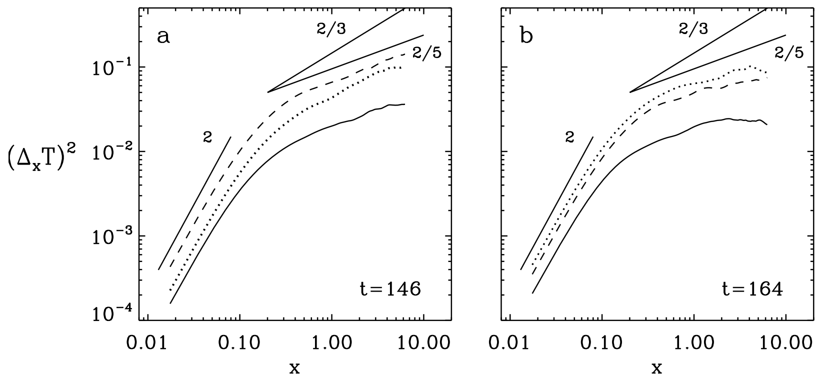


Figure 4: Second-order temperature structure functions at mid-layer (solid) and midway between the middle of the layer and the top (dotted) and bottom (dashed) edges at (a) $t = 146$ and (b) $t = 164$. The $r^2$ law as $r \to 0$ is demonstrated. The $r^{2/3}$ law for isotropic turbulence (Kolmogorov) and the $r^{2/5}$ law for stratified turbulence (Bolgiano) are also indicated. Despite the good agreement with the $r^{2/5}$ law, we do not believe Bolgiano's theory applies (see text).

As the preceding analysis demonstrates, stratified shear turbulence exhibits anisotropy on all scales of motion. This includes even the smallest, dissipative scales. Both mean shear and buoyancy introduce directionality into the flow statistics, spoiling the possibility of isotropy. Clear signatures in the large-scale distribution of $n$ (index of refraction) are predicted (see Fig. 1 and accompanying discussion). The spacing and extent of such strong $n$ layers will be addressed in future and on-going work.

The tendency toward greater relative stratification inside the shear layer near the layer edges at $t = 146$ and throughout the layer at $t = 164$ suggests a possible change in spectral character. Fig. 4 demonstrates this by plotting the temperature structure function $(\Delta_r T)^2$ at mid-layer and midway between the center of the layer and the layer's edges. For isotropic turbulence with a $k^{-5/3}$ inertial range, $(\Delta_r T)^2 \propto r^{2/3}$, which is close to the value observed for only one of the curves (dotted) in Fig. 4a. The remaining curves in 4a,b exhibit a $r^{2/5}$ law, which is consistent with Bolgiano's $k^{-7/5}$ prediction for buoyancy-dominated, anisotropic turbulence. Bolgiano's theory assumes axisymmetry about the vertical direction and independence of the spectral shapes on the eddy-kinetic-energy flux on the spectra, two assumptions which are violated by the numerical solutions. Furthermore, Bolgiano's theory predicts a much steeper $k^{-11/5}$ slope for velocity spectra, which we do not observe. Clearly, more work is required to understand the $r^{2/5}$ laws we observe.

## References

1. Spalart, P.R., R.D.Moser and M.M.Rogers, "Spectral methods for the Navier-Stokes equations with one infinite and two periodic directions," J. Comput. Phys., Vol 96, pp.297–324, 1991.

2. Werne, J. and D.C.Fritts, "Turbulence in Stratified and Sheared Fluids: T3E Simulations" HPCMO Users Group Conference, Ed. N. Sidki, Rice University, Houston, TX. June 1998, http://www.hpcmo.hpc.mil/Htdocs/UGC/UGC98/papers/1f_chal/index.htm

3. Werne, J. and D. C. Fritts, "Stratified shear turbulence: Evolution and Statistics" (cover article) Geophys. Res. Lett., Vol 26, pp.439–442, 1999a.

4. Werne, J. and D. C. Fritts, "Turbulence and Mixing in a Stratified Shear Layer: 3D K-H Simulations at $Re = 24,000$" European Geophysical Society, XXIV General Assembly. April 1999, The Hague, 1999b.

5. Ierkic, H. M., R. F. Woodman and P. Perillat, "Ultrahigh vertical resolution radar measurements in the lower stratosphere at Arecibo," Radio Sci., Vol 25, pp.941–952, 1990.

6. Hinze, J. O., "Turbulence" McGraw-Hill, New York, 1959.

7. Monin, A. S. and A. M. Yaglom, "Statistical Fluid Mechanics, Vol 2" MIT Press, Cambridge, 1975.

8. George and Hussein, "Locally axisymmetric turbulence" J. Fluid Mech., Vol 233, pp.1–23, 1991.